Nanoscale

ROYAL SOCIETY OF CHEMISTRY

PAPER

View Article Online
View Journal | View Issue

Cite this: *Nanoscale*, 2023, **15**, 6343

Ultra-sensitive graphene membranes for microphone applications†

Gabriele Baglioni, *[a] Roberto Pezone,[b] Sten Vollebregt,[b] Katarina Cvetanović Zobenica, [c] Marko Spasenović, [c] Dejan Todorović,[d] Hanqing Liu,[e] Gerard J. Verbiest,[e] Herre S. J. van der Zant [a] and Peter G. Steeneken*[a,e]

Microphones exploit the motion of suspended membranes to detect sound waves. Since the microphone performance can be improved by reducing the thickness and mass of its sensing membrane, graphene-based microphones are expected to outperform state-of-the-art microelectromechanical (MEMS) microphones and allow further miniaturization of the device. Here, we present a laser vibrometry study of the acoustic response of suspended multilayer graphene membranes for microphone applications. We address performance parameters relevant for acoustic sensing, including mechanical sensitivity, limit of detection and nonlinear distortion, and discuss the trade-offs and limitations in the design of graphene microphones. We demonstrate superior mechanical sensitivities of the graphene membranes, reaching more than 2 orders of magnitude higher compliances than commercial MEMS devices, and report a limit of detection as low as 15 dB_{SPL}, which is 10–15 dB lower than that featured by current MEMS microphones.

Received 19th September 2022,
Accepted 8th March 2023

DOI: 10.1039/d2nr05147h

rsc.li/nanoscale

Introduction

MEMS microphone technology, based on Si manufacturing processes, has benefited from the proliferation of portable electronic devices, experiencing unprecedented market growth[1] (reaching around 8 billion sold units in 2022) as well as continuous design and production improvements.[2,3] One of the main device development targets is the optimization of the mechanical sensitivity, which determines the microphone's ability to pick up sound. The mechanical sensitivity, defined as the membrane's displacement amplitude per unit sound pressure, scales inversely with the thickness and stress of the sensing membrane.[2] Complex fabrication techniques involving corrugated membranes[4,5] or not-fully supported membranes[6–8] have been implemented to reduce residual fabrication stress and boost sensitivity of thin MEMS membranes.

Being ultrathin and lightweight, suspended graphene membranes are excellent candidates for use in electrostatically actuated devices[9–11] and sensors,[12] such as pressure sensors,[13–15] gas sensors[16] and accelerometers[17] as well as microphones.[18–25] Thanks to their atomic thickness, graphene membranes could be made more than a factor 100–1000 times thinner than typical 0.1–1.0 μm thick MEMS membranes, resulting in a significant increase of the microphone mechanical sensitivity without requiring complex device structures. On top of that, graphene is an excellent conductor and thus requires no additional layer for electrical readout. Previous studies have demonstrated the fabrication of microphones using graphene-based membranes either with multilayer graphene[18–20] or with a composite structure made of bilayer or multilayer graphene and a thick (>100 nm) PMMA layer.[21–25] In general, these works focused on fabricating a condenser microphone structure, involving either wet or dry transfer[20–22] of large graphene membranes (from 2 to 12 mm in diameter) over pre-patterned substrates or *via* dry etching of a sacrificial

[a]*Kavli Institute of Nanoscience, Delft University of Technology, The Netherlands. E-mail: G.Baglioni@tudelft.nl, P.G.Steeneken@tudelft.nl*
[b]*Laboratory of Electronic Components, Technology and Materials, Delft University of Technology, The Netherlands*
[c]*Center for Microelectronic Technologies, Institute of Chemistry, Technology and Metallurgy, University of Belgrade, Serbia*
[d]*Dirigent Acoustics Ltd, Belgrade, Serbia*
[e]*Department of Precision and Microsystems Engineering, Delft University of Technology, The Netherlands*

† Electronic supplementary information (ESI) available: Fig. S1: Raman spectrum of graphene samples; Fig. S2: AFM characterization of graphene samples; Fig. S3: Mechanical sensitivities at 1 kHz of all measured samples: Fig. S4: Measurements of resonance frequency in vacuum and comparison with resonance in air; Fig. S5: Effects of wrinkles on membrane's mode shape; Fig. S6: SEM pictures of graphene membranes; Fig. S7: Mechanical compliance corrected by resonance frequency; Fig. S8: Growth and transfer process of the graphene membranes; Movie V1: LynceeTec mode shape imaging of graphene membrane; Movie V2: LynceeTec mode shape imaging of wrinkled graphene membrane; Audio A1: music track (Ode to joy) recorded on optically on multilayer graphene membrane. See DOI: https://doi.org/10.1039/d2nr05147h

layer.[23] In these devices, the incoming sound is transduced to an electrical signal *via* the change in capacitance between a fixed backplate and the movable membrane. Although these works have demonstrated successful capacitive readout of audio signals with high output voltage per unit pressure, other important device performance parameters, like the mechanical sensitivity, the signal-to-noise ratio (SNR), total harmonic distortion (THD), bandwidth and dynamic range, have been less extensively characterized. Following common conventions for microphone specifications, we define these parameters using the reference input frequency and reference pressure level as 1 kHz and 1 Pa = 94 dB_{SPL} respectively:

- **Sensitivity**: ratio between electrical output and input sound pressure, usually expressed in mV Pa^{-1} for capacitive microphones. This overall sensitivity is a combination of *electrical sensitivity*, which depends on the readout-circuit and amplification, and *mechanical sensitivity*.[2] In this work, we address the mechanical sensitivity, given by the ratio between membrane's displacement and input pressure which strongly depends on the material properties and membranes dimensions.
- **Signal-to-noise ratio (SNR)**: ratio between output in response from a reference signal (1 kHz at 1 Pa) and noise level of the microphone.
- **Dynamic range**: difference between the maximum and minimum sound pressure level that the microphone can handle. The maximum detectable sound is determined by the amount of nonlinear distortion in the microphone response.
- **Total harmonic distortion (THD)**: measures the level of distortion at the output and it is defined as the ratio between the sum of the powers of the harmonics and the fundamental tone. Maximum detectable sound is determined by the acoustic overload point (AOP) corresponding to THD = 10%.

In this work, we use a Laser Doppler Vibrometer (LDV) to carry out a detailed study of the response of multilayer graphene (MLG) membranes to acoustic actuation, and determine their most important performance parameters such that they can be compared to the stateof-the-art. The advantage of optical vibrometry is that it allows direct determination of the mechanical response of graphene membranes to sound, in contrast to electrical methods, where the output voltage depends on the specifics of the readout circuit. Moreover, by using it to characterize freestanding membranes, it allows measurement of the intrinsic membrane characteristics without including effects of a backplate that is used in capacitive condenser microphones. Thus, we gain deeper insights into graphene's acoustic properties, which is crucial for the design of future MEMS graphene microphones.

Experimental section

Fig. 1a shows the schematic of the setup used to characterize the multilayer graphene membranes. A single-point Laser Doppler Vibrometer LDV (OFV-5000 vibrometer controller and OFV-534 fiber-coupled vibrometer sensor head) is used to measure the displacement at the centre of the membrane. A reference microphone (Sonarworks XREF20), placed below the sample under study, detects the input sound pressure level from a commercially available speaker used to acoustically actuate the graphene membrane. The displacement signal is reconstructed by the DD-900 decoder of the vibrometer controller with responsivity, R_{LDV} set between 100 nm V^{-1} and 1 μm V^{-1}. The spectrum analyzer and frequency response analyser functions of Moku:Lab Field Programmable Gate Array (FPGA) based signal generator and analyzer are used to

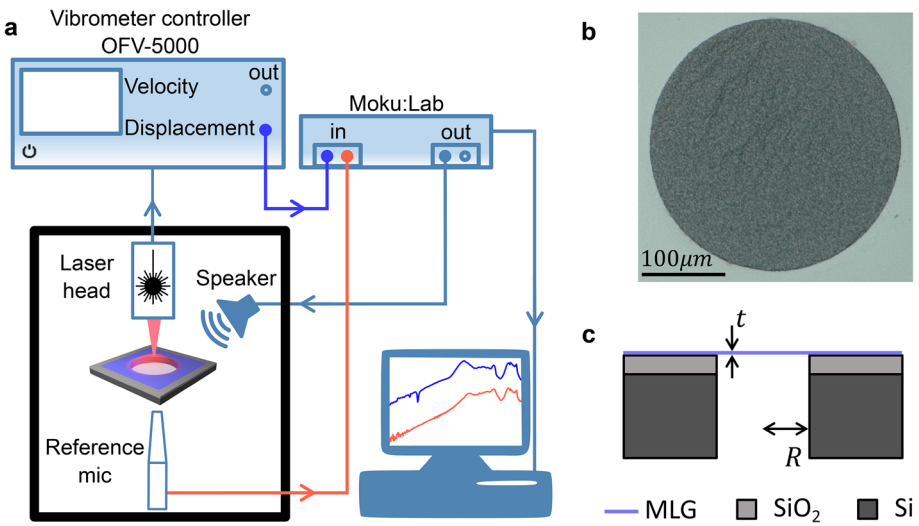

Fig. 1 Experimental setup and samples. (a) Schematics of the experimental setup. The vibrometer measures the dynamic motion of the graphene membrane as a result of the sound from a speaker at a distance of ~2 cm, while a reference microphone, that is mounted within ~5 mm below the chip, detects the sound level at the sample location. Measurements are controlled *via* the Moku:Lab using the spectrum analyzer and frequency response analyser functions. The setup is placed inside a sound proof box. (b and c) Optical image and schematic cross section of a multilayer graphene membrane (thickness t ~8 nm) transferred over a through-hole with a diameter $d = 2R$ = 350 μm in a Si/SiO_2 substrate.

measure the displacement signal from the vibrometer and sound pressure signal from the microphone as well as controlling the driving signal to the speaker.

A soundproof box encloses the setup to reduce influence of background noise.

An optical picture of a typical graphene membrane and its schematic cross-section are shown in Fig. 1b and c. The free-standing membranes are made of multilayer graphene with a thickness of ~8 nm grown on Si/SiO_2/Mo (50 nm) by Low-Pressure Chemical Vapor Deposition in an Aixtron Black Magic reactor at 1000 °C with H_2–CH_4 as carbon precursor source. The Mo seed layer under the graphene is wet-etched with H_2O_2 and deionized water, after which the graphene remains on the Si/SiO_2 substrate.[26] The graphene is finally immersed in DI-water until it delaminates and it is carefully wet-transferred on a Si/SiO_2 substrate (thickness of ~520 μm) with pre-patterned holes. These holes, with a diameter of ~350–600 μm were etched through the silicon chips by Deep Reaction Ion Etching (DRIE) and buffered oxide etch (BOE) to remove the SiO_2 hard mask. Finally, the chip with suspended graphene membranes is dried in atmospheric conditions for >10 hours.

The graphene used in this study has been found to be strong enough to sustain drying in atmospheric conditions, without a need for critical point drying. The high mechanical quality of the graphene is related to its high uniformity.[27] Furthermore, the membranes are completely freely suspended over the through holes, which alleviates the possibility of liquid formation between the graphene and the substrate. The crystallinity of the graphene as well as its thickness were investigated *via* Raman and atomic force microscopy (see Fig. S1 and S2 in the ESI†).

Results

We investigate the acoustic spectrum of the graphene membranes by measuring their centre displacement in response to an acoustic chirp from 200 Hz to 20 kHz. Owing to frequency limitation of the speaker used, our setup did not enable accurate characterization of the membranes at frequencies below 100 Hz. Fig. 2a shows typical frequency responses from the LDV (in blue) and from the reference microphone (in red). The reference signal (in red) is measured before placing the sample on the reference microphone, in order to avoid any shading of the sound from the speaker. The vibrometer outputs a voltage signal V_{LDV} proportional to the membranes displacement, z, where $V_{LDV} = zR_{LDV}$. Similarly, the output voltage of the reference microphone is proportional to the incoming sound pressure level by its calibrated sensitivity in the audible range. After correcting for the vibrometer's responsivity (in nm V^{-1}) and for the calibrated sensitivity of the microphone (in mV Pa^{-1}), the ratio of the two voltage signals in Fig. 2a yields the mechanical sensitivity in nm Pa^{-1} of the graphene membrane, which is shown in Fig. 2b.

Following this methodology, we characterize the acoustic response of multilayer graphene membranes of varying diameters, as well as the membrane of a commercial MEMS microphone from ST-Microelectronics (MP23DB01HP), and compare their performance. To avoid confusion with other MEMS devices from literature, the commercial device is referred to as 'ST MEMS microphone' in the rest of the manuscript. In Fig. 3a, the frequency response of four graphene drums with a diameter d = 350 μm is shown together with the response of the ST MEMS microphone (d = 950 μm). Also, the mechanical sensitivity at 1 kHz ($S_{m,1\ kHz}$) of the 37 measured drums is shown in Fig. S3 of the ESI.†

This quantity is defined as $S_{m,1\ kHz} = \frac{\Delta z_{1\ kHz}}{\Delta P_{1\ kHz}}$ where $\Delta z_{1\ kHz}$ is the AC amplitude of the membrane centre at 1 kHz and $\Delta P_{1\ kHz}$ is the input sound pressure amplitude at 1 kHz. Even though large differences in sensitivity between graphene membranes are observed, all graphene membranes exhibit much higher mechanical sensitivities (up to ~2000 nm Pa^{-1}) than the ST MEMS microphone with $S_{m,1\ kHz}$ ~1.3 nm Pa^{-1}.

To analyze these results, the data points in Fig. 3a were fit (drawn lines) using a harmonic oscillator model,

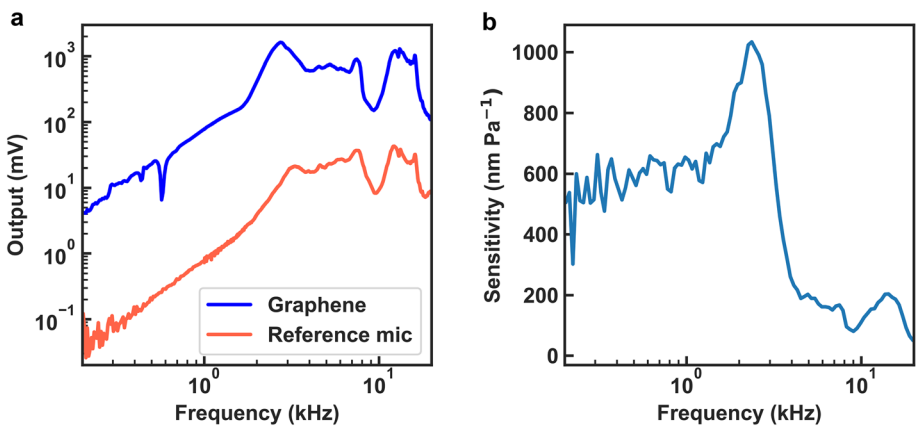

Fig. 2 Frequency response measurements. (a) LDV displacement data (blue line) of a graphene membrane (diameter d = 350 μm) and sound pressure data (light red line) recorded by the reference microphone between 200 Hz and 20 kHz. (b) Mechanical sensitivity of the membrane, as determined from (a).

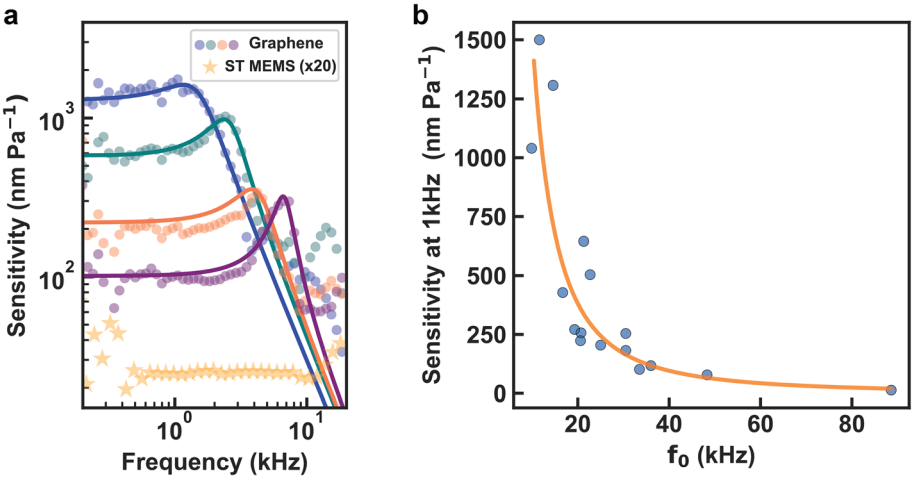

Fig. 3 Sensitivity in the audible spectrum. (a) Audio response spectra of graphene membranes (d = 350 μm) and the Si membrane in the ST MEMS microphone. Drawn lines are fits to the data using a harmonic oscillator model. (b) Acoustic sensitivity of 16 different graphene membranes with d = 350 μm at 1 kHz plotted against the fundamental resonant frequency f_0 measured in vacuum with a scanning LDV (as discussed in detail in section 3 of the ESI†). Differences in resonance frequency and sensitivity are attributed to variations in pretensions induced by the transfer process.

yielding a frequency dependent mechanical sensitivity $S_m(\omega)$

$$S_m(\omega) = \frac{R^2}{4n_0\sqrt{(1-\omega^2/{\omega_0}^2)^2 + \omega^2/({\omega_0}^2 Q^2)}}, \quad (1)$$

where n_0 is the initial pretension in the membrane, R is the membrane radius, Q is the quality factor and $f_0 = \omega_0/(2\pi)$ the fundamental resonance frequency corresponding to peaks in the curves in Fig. 3a. The low-frequency response ($\omega \ll \omega_0$), $S_m(0) = \frac{R^2}{4n_0}$, can be calculated using the equation for the static displacement, z, of a circular membrane subjected to a uniform pressure load ΔP:[15]

$$\Delta P = \frac{4n_0}{R^2}z + \frac{8E_t}{3R^4(1-\nu)}z^3, \quad (2)$$

where E is Young's modulus and ν is the Poisson's ratio of the material. Thus, in the limit of small z, the mechanical sensitivity of the membrane can be expressed as $S_m(0) \approx \frac{z}{\Delta P} = \frac{R^2}{4n_0}$. Even though it has a two to three times smaller diameter than the ST MEMS microphone, the mechanical sensitivity of the graphene membrane is extremely large thanks to its low pretension n_0.

According to eqn (1), the main parameter determining $S_m(0)$ is the pretension. Thus, variation in sensitivity observed between the devices in Fig. 3 is likely due to fabrication induced differences in pretension. To check this hypothesis, we consider the equation for the fundamental resonance frequency, f_0, of a circular membrane and its relation to the mechanical sensitivity $S_m(0)$:

$$f_0 = \frac{2.405}{2\pi R}\sqrt{\frac{n_0}{\rho_{eff}t}} = \frac{2.405}{4\pi}\sqrt{\frac{1}{S_m(0)\rho_{eff}t}}, \quad (3)$$

where ρ_{eff} is the effective density of the membrane, which can be affected by air loading effects (see section 3 of the ESI†). Since 1 kHz is below the resonance frequency of the membrane, $S_{m,1\ kHz} \approx S_m(0)$. Therefore, we expect to observe the following proportionality relation between mechanical sensitivity and resonance frequency: $S_m \propto {f_0}^{-2}$.

To remove the influence of air loading effects on the resonance frequency, we also measure the membranes' resonance frequency in vacuum using a scanning laser Doppler vibrometer (MSA400 Micro System Analyzer). The sample is placed inside a vacuum chamber (~10^{-3} mbar) equipped with a piezo shaker to actuate the membrane. The displacement is measured over a user-defined grid of points distributed over the surface of the membrane. Thus the membrane mode shape can be reconstructed to identify the first resonance mode (see section 3 of the ESI for more details†).

In Fig. 3b we plot the sensitivity at 1 kHz against f_0 measured using a scanning LDV in vacuum. The data in Fig. 3b follows the theoretically expected relation $S_m \propto {f_0}^{-2}$, showing that the experimental differences in sensitivity observed in Fig. 3b can indeed be well accounted for by variations in n_0. Fig. S3b in the ESI,† shows correlations between mechanical sensitivity and resonance frequencies measured in air from data like in Fig. 3a. Variations in pretension can be caused by forces on the graphene during the transfer process, and might also be induced by wrinkles in the membranes (see Fig. S5 in the ESI†).

A high sensitivity does not automatically guarantee that a microphone can detect weak sounds, because its limit of detection (LOD) also depends on the noise level. To determine the LOD, we measured the membrane displacement at 1 kHz for different driving amplitudes to investigate the minimum detectable sound pressure level (SPL). Fig. 4a shows the displacement signal from the vibrometer in response to a 1 kHz tone at low SPL (<35 dB_{SPL}) for the ST MEMS microphone and three

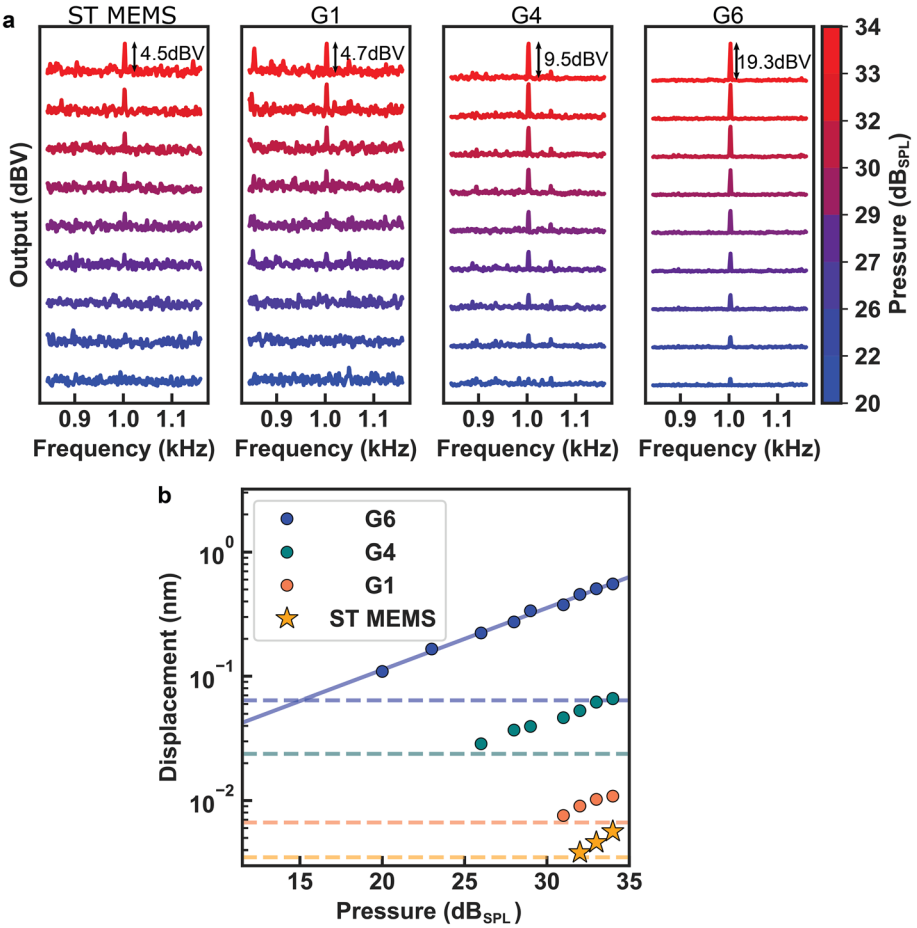

Fig. 4 Minimum detectable SPL. (a) Waterfall plot of the displacement amplitudes for three graphene drums and the ST MEMS microphone in response to a 1 kHz tone at low input sound pressure levels (20–34 dB_{SPL} indicated by colour scale). The most sensitive graphene membrane G6 detects sounds down to 20 dB_{SPL} with SNR = 5 dB. (b) Extracted peak amplitudes at 1 kHz from Fig. 4(a) of the four samples. The dashed lines show the average noise level (NL) of the corresponding samples. Peaks with amplitudes smaller than 1.1 × NL were removed from the plot. A linear fit through the points from device G6 is also shown to determine the minimum detectable SPL by extrapolation (LOD ~15 dB_{SPL}).

graphene membranes with different mechanical sensitivity (labelled as G1, G4, G6) and d = 350 μm. The vibration amplitude at 1 kHz as a function of the input SPL, as obtained from the peak heights in Fig. 4a using the vibrometer responsivity of 200 nm V^{-1}, is shown in Fig. 4b for the four devices. The measured average noise level for each sample is depicted with a dashed line of the corresponding colour. For SPL > 30 dB_{SPL}, the response peak at 1 kHz is visible in all samples with varying amplitudes depending on the sample's mechanical sensitivity. When decreasing the input SPL, the 1 kHz peak becomes comparable to the noise level at ~30–32 dB_{SPL} for the ST MEMS microphone and G1, while for G4 and G6 the extrapolated signal stays above the noise level down to 25 and 15 dB_{SPL} respectively, which is significantly lower than the lowest SPL of 70 dB_{SPL} at which graphene membranes were tested in literature[21] up to now. The extrapolated LOD of ~15 dB_{SPL} of device G6 is even lower than the specified LOD of the reference microphone of 24 dB_{SPL} used to measure the input SPL.

Fig. 4b shows that the noise level increases when the sensitivity increases due to a smaller stiffness k, because the thermomechanical noise induces a mean displacement given by: $< x^2 >= \frac{k_B T}{k}$.[28] The thermomechanically induced displacement power spectral density below resonance $S_{xx,n} = \frac{4k_B T}{kQ\omega_0}$ can be calculated by extracting k from a linear fit to Fig. 5b and Q and ω_0 from a harmonic oscillator fit to the resonances in air, leading to a theoretical value of the thermomechanical noise displacement density ${}^{P}S_{xx,n}$ of ~8, 1.8, 0.2 pm Hz^{-1} for sample G6, G4, G1 respectively. The noise level measured is ~47, 17, 5 and 3 pm Hz^{-1} for sample G6, G4, G1 and the ST MEMS respectively, showing that the displacement noise in the membranes is near, but not at the theoretical limit.

To determine the microphone performance at high sound pressure levels, similar measurements were performed at high SPL to study the dynamic range, the distortion and nonlinearity of the response. In Fig. 5a we show the response amplitude

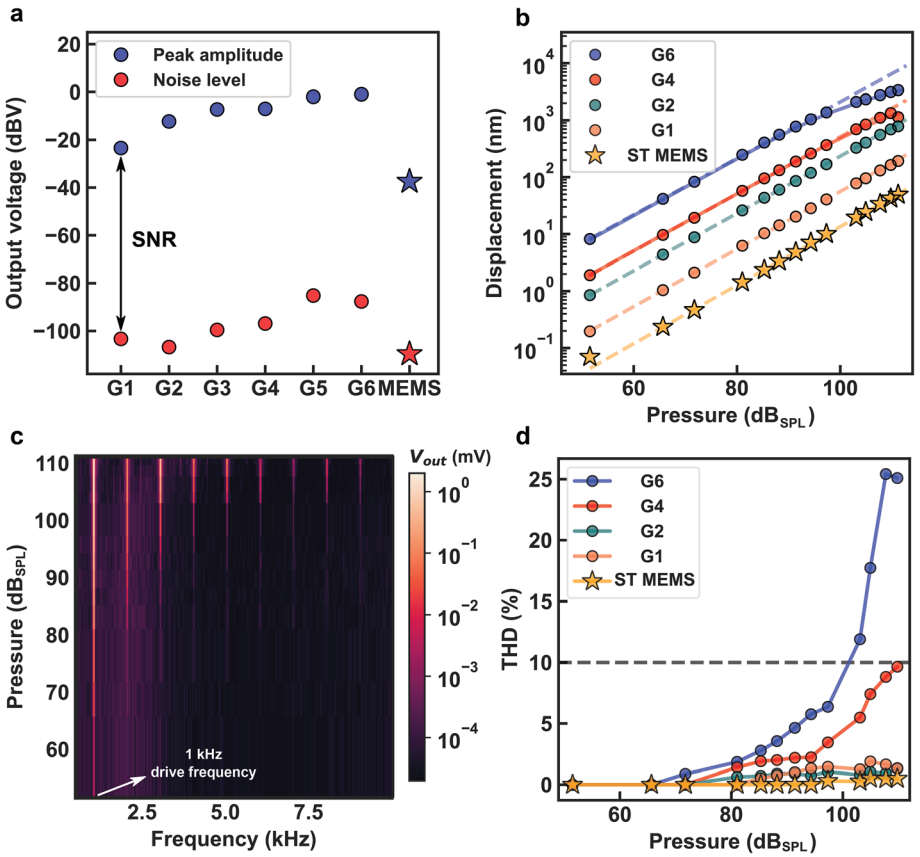

Fig. 5 Signal-to-noise ratio and harmonic distortion. (a) Comparison between displacement signal from graphene membranes (circles) and from the ST MEMS microphone (stars) in response to a 1 kHz tone at 1 Pa of rms SPL (= 94 dB$_{SPL}$). The blue markers indicate the peak amplitude while the red markers indicate the noise floor of the spectra (like in Fig. 4a). Average SNR in graphene is 88 dB, 16 dB higher compared to that of the ST MEMS microphone. (b) Displacement amplitude at 1 kHz *vs.* SPL for several graphene drums and the ST MEMS microphone, extracted from spectra like in Fig. 4a. (c) Displacement spectrum of device G6 as a function of SPL of a 1 kHz tone from the speaker. (d) Total harmonic distortion (THD) *versus* SPL for the samples in 5b. The dashed line at THD = 10% marks the acoustic overload point (AOP).

as well as the average noise level of some membranes to a 1 kHz tone of 1 Pa (= 94 dB$_{SPL}$) to compare their signal-to-noise ratio $SNR_{1\ Pa,1\ kHz} = x_{1\ Pa,1\ kHz}/^{p}S_{xx,n}$ to that of the ST MEMS microphone. On average, the noise level of the graphene membranes is higher compared to that of the ST MEMS microphone. However, due to their higher sensitivity at 94 dB$_{SPL}$, the SNR (difference between blue and red data points in Fig. 5a) of the graphene microphones ranges from 80–95 dB, which is significantly larger than that of the ST MEMS microphone, which is 72 dB.

In Fig. 5b, we show the peak amplitude of the displacement signal in response to a 1 kHz tone between 50 dB$_{SPL}$ and 110 dB$_{SPL}$. Louder acoustic signals were not used due to large distortion and clipping occurring in the speaker. All graphene samples exhibit a higher response than the ST MEMS microphone, but at a high SPL the most sensitive samples deviate from linear behaviour. This is to be expected as the linear approximation of eqn (2) holds in the limit of small displacements. Therefore, while sample G6 was the best at detecting low sound levels down to 20 dB$_{SPL}$, its performance at high SPL gets worse due to non-linear effects limiting its dynamic range. The non-linear response of G6 and G4 was fitted to eqn (2) with t = 8 nm, $2R$ = 350 μm and ν = 0.26 yielding a pretension n_0 ~7 mN m^{-1} and 33 mN m^{-1} and a Young's modulus of E ~5 GPa and 30 GPa for G6 and G4 respectively. The extracted Young's modulus is much lower than that of pristine graphene. This reduction could be due to defects that originate from graphene growth in the form of small holes of ~50 nm, as observed by SEM inspection of the samples (see Fig. S6 in ESI†). In addition, transfer-induced wrinkles and slack in the membrane can further decrease the Young's modulus.[29]

To analyze the observed distortion, the spectrum of sample G6 in response to a 1 kHz tone with varying SPL at 1 kHz is shown in Fig. 5c. At higher SPL, harmonics of the driving frequency are visible in the spectrum. In order to measure the distortion level and maximum detectable SPL of the samples under study, we calculated the THD from the first five harmonics as:[30]

$$\mathrm{THD} = \frac{\sqrt{\sum_{i>0} V_i^2}}{V_0} \quad (4)$$

where V_i is the rms voltage output at the i-th harmonic ($i > 0$) and V_0 is the output at the driving frequency. The maximum SPL that a microphone can handle is determined by the acoustic overload point (AOP), which is usually defined as the pressure level at which the THD reaches 10%.[30] The dynamic range is then given by the difference in dB between the AOP and minimum detectable SPL, which for MEMS devices is usually determined by the microphone's noise level. In the calculation of the THD of the membrane's displacement, contributions from harmonics generated by the speaker were subtracted. The extracted THD as a function of the input SPL is shown in Fig. 5d. Samples G6 and G4 reach the acoustic overload point at around 98 dB_{SPL} and 110 dB_{SPL} respectively, setting their dynamic range to ~83 dB and 87 dB. The other samples are well below the AOP at the maximum SPL applied so that their dynamic range is >85 dB. The measured THD at 110 dB_{SPL} of the ST MEMS microphone is ~0.5%, in close agreement with the reported THD in its datasheet.[31]

In order to theoretically estimate the expected value of the THD, we assume periodic motion of the membrane $z(t) = z_0 \sin \omega t$, which when substituted in eqn (2) yields

$$\Delta P(t) = \left(\alpha z_0 + \frac{3}{4}\beta {z_0}^3\right) \sin \omega t - \frac{\beta}{4} {z_0}^3 \sin 3\omega t, \quad (5)$$

where $\alpha = \frac{4n_0}{R^2}$ and $\beta = \frac{8E_t}{3R^4(1-\nu)}$. Using values of n_0 and E from the fit to the non-linear response curves in Fig. 5b, we calculate the expected distortion just from the third harmonic as: $\mathrm{THD}^{3rd} = \frac{\beta {z_0}^2}{4\alpha + \beta {z_0}^2}$. The resulting THD_{3rd} for samples G6 and G4 at the maximum applied SPL of 110 dB_{SPL} is 21.5% and 7.5% respectively. This is consistent with the measured values of 25% and 9.6% corresponding to THD from the first 5 harmonics, since the third harmonic is expected from eqn (2) to have the largest contribution to the THD.

Discussion

We have established that graphene membranes can offer very high acoustical sensitivities that are up to two orders of magnitude higher than that of MEMS microphones. In commercial applications, a microphone's signal is usually detected electrically *via* capacitive readout. In the capacitive configuration, the microphone's ability to pick up sound is described by its open circuit sensitivity, S, namely the ratio of the microphone's open circuit output voltage over the driving SPL in Pa. The open circuit sensitivity is given by the product of the microphone's electrical S_e and mechanical S_m sensitivities as:[32]

$$S = S_e S_m = \frac{V_b}{g_0} S_m, \quad (6)$$

where V_b is the bias voltage and g_0 is the equilibrium gap distance between the capacitor plates. Using this formula we can further compare our membranes with MEMS devices reported in literature[2] by extracting their mechanical sensitivity S_m from published values of S, V_b and g_0 using eqn (6). To have a more direct comparison between devices of different geometries/dimensions, we divide the mechanical sensitivity by the area of the membrane which yields the membrane's mechanical compliance, C_m.

Fig. 6 shows the mechanical compliance as a function of membrane thickness for MEMS devices reported in ref. 2 (blue circles), for graphene-based microphones (red and purple hexagons), and for the multi-layer graphene (MLG) membranes presented here (green hexagon). The data points shown for the MLG membranes of our work include the membranes with highest and lowest compliance to highlight the range of measured values compared to previous reports in literature. The compliance of graphene-based membranes not listed in ref. 2 is estimated from the reported membrane pretension using $C_m = \frac{1}{k}$, where the membrane's stiffness $k = 4\pi n_0$ in the case of pressure deformation.[33] Moreover, since $n_0 = \sigma t$ where σ is the pre-stress of the membrane, we can identify lines of constant stress in the C_m *vs.* t plane. These are highlighted as dashed red lines in Fig. 6 with lower stress corresponding to lower opacity of the line. The high mechanical sensitivity of our membranes can thus be attributed to a combination of low stress and small thickness. The high stress reported on the t = 25 nm membrane in ref. 20 results from the large polarization voltage of 200 V used to readout the acoustic signal, which led to an estimated pretension of 640 N m^{-1}.

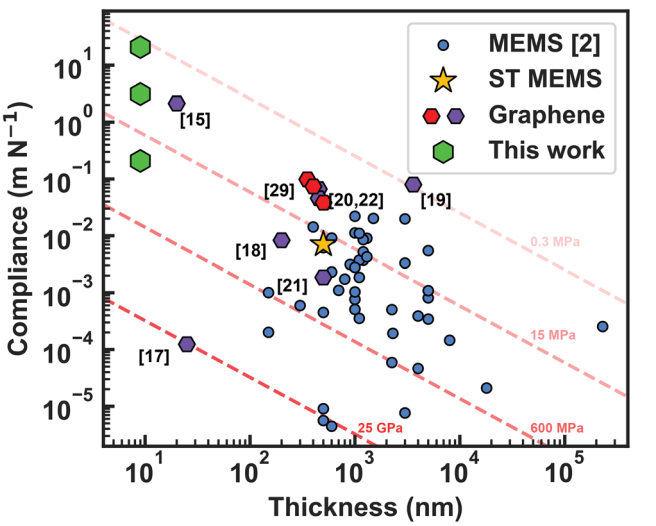

Fig. 6 Mechanical compliance of literature devices. Scatter plot of mechanical compliance *vs.* membrane's thickness for MEMS microphones from literature[2] (blue circles), the ST MEMS microphone (yellow star), graphene microphone literature (purple and red hexagons for membranes with and without a backplate respectively) and for three graphene membranes in this work (green hexagon), including membranes with lowest and highest compliance measured. The dashed red lines indicates lines with constant stress, with lower stress corresponding to lines with lower opacity. The relevant reference numbers for the graphene microphones are indicated in the graph near the data points.

We note that most microphone works in literature deal with membranes with a backplate for capacitive readout. Therefore, the lower compliance in these devices (at atmospheric pressure) can be partly explained by the effect of squeeze film damping. The graphene membranes under study do not have such a backplate, because we first wanted to determine the intrinsic properties of the graphene membranes themselves. Realizing efficient electrical microphone readout, *e.g. via* a perforated capacitive backplate, while maintaining this high sensitivity and compliance is another challenge that is outside the scope of this work.

Although lowering the tension and stiffness of graphene membranes helps to improve their acoustic sensitivity, a drawback is that it reduces the fundamental resonance frequency, thus limiting the microphone bandwidth (Fig. 3b). Since the mass of the graphene membranes is extremely low, and their aspect-ratio very high (d/t ~46 000), the mass of the air that moves along with the membrane is substantial, increasing the effective membrane mass m_{eff}.[34,35] This mass increase further reduces the resonance frequency and bandwidth. Initial experiments showed a 5 to 9-fold decrease of the resonant frequency from vacuum ~10^{-4} mbar to atmospheric conditions (see Fig. S4 in the ESI†). Further pressure-dependent measurements are needed to understand better this air mass loading effect as well as the importance of squeeze-film damping on future devices with backplate for capacitive readout.

In general, it is desirable to have the resonance frequency of the membrane above the audible range (>20 kHz). The membranes in this work, like in several other graphene microphone publications,[18,22,23] do not satisfy this condition. However, it is important to note that depending on the target application, a bandwidth of 6–10 kHz can be sufficient,[22,36] therefore the reported low resonance frequency (<10 kHz) of graphene membranes is not necessarily limiting for their performance. Nevertheless, this problem could be compensated for in next generation devices by increasing their pretension n_0 or reducing the membrane radius R, while keeping competitive mechanical sensitivity. For example, as shown in ref. 37 graphene membranes with diameters of 85–150 μm exhibit resonance frequencies in vacuum of 250–320 kHz and mechanical sensitivities still comparable to a MEMS membrane with a diameter of 950 μm. For a fairer comparison, one can correct the obtained compliances in Fig. 6 by a factor $(20\ \mathrm{kHz}/f_0)^2$. Even after such a correction, the compliances obtained by the graphene membranes in this work are higher than most literature values as shown in Fig. S7 in the ESI.†

A main challenge in using graphene as a microphone is linked to the lack of control over its mechanical properties during the transfer process, which limits the reproducibility of the membrane's performance as shown in Fig. 3 and Fig. S3.† For microphone applications, large sheets of suspended CVD graphene are needed and thus a transfer step to the target substrate has been unavoidable in all previous studies. In addition to the poor uniformity and control of strain, the transfer process can degrade the quality of the graphene by introducing contamination, cracks and wrinkles, unwanted for practical application and large-scale production.[38] In a recent study,[37] wafer-scale fabrication of multilayer graphene membranes was achieved using a transfer-free method, by which the graphene is grown and released directly on the target substrate. This novel method could prove beneficial in terms of uniformity and scalability in fabrication of graphene-based microphones and sensors.

Finally, the most sensitive membranes are found to be more influenced by non-linear effects at high SPL, and exhibit higher distortion and reduced dynamic range. Graphene membranes cannot yet reach commercial values of THD, acoustic overload point (AOP = 140 $\mathrm{dB_{SPL}}$) and dynamic range (105 $\mathrm{dB_{SPL}}$[31]), also because they do not feature a doublebackplate configuration for differential readout which greatly reduces the THD and increases sensitivity.[36] The trade-off between sensitivity and dynamic range could be further optimized by better control over the membrane's stiffness.

Conclusions

In this work, evidence is provided that, with proper design, graphene-based devices have the potential to outperform existing microphones. In terms of mechanical sensitivity and SNR, graphene is superior to commercial Si-based membranes and MEMS devices from literature by a large margin, yielding an improvement of more than 2 orders of magnitude in sensitivity. In addition we show that the detection limit of graphene membranes is as low as 15 $\mathrm{dB_{SPL}}$ for membranes with a diameter of only 350 μm. On the other hand, due to the low stiffness and the large contribution of air loading, the membrane's bandwidth is found to be limited at <10 kHz on most samples. However, we show that even when taking this factor into account, the membranes in this work are still more performant than commercial devices. We propose that given the high sensitivity of graphene one can further reduce the sensor's dimensions, increasing its resonance frequency, bandwidth and mechanical strength. Smaller sized membranes would also facilitate the implementation of arrays of membranes in parallel to increase SNR[36] or directionality and reduce effects of added air as well as squeeze film damping in closed cavity resonators with capacitive readout.[39] Therefore, we believe that graphene can indeed improve current microphone devices and that the main disadvantage and barrier to real applications lies in the lack of a more controllable fabrication method to suspend graphene membranes.

Author contributions

G. B., H. S. J. v. d. Z. and P. G. S. conceived the experiments. G. B. performed the experiments. R. P. and K. C. fabricated and inspected the samples. G. B., G. J. V., H. L., and P. G. S. analyzed and modeled the experimental data. G. B wrote the manuscript with contributions from all the authors. H. S. J. v. d. Z., M. S., D. T., G. J. V., S. V. and

P. G. S. revised the manuscript. H. S. J. v. d. Z., M. S., S. V. and P. G. S. supervised the project.

Data availability

The data that support the findings of this study are available from the corresponding authors upon request.

Conflicts of interest

The authors declare no competing interests.

Acknowledgements

The authors acknowledge funding from European Union's Horizon 2020 research and innovation program under Grant Agreement No, 881603 (Graphene Flagship) and No. 883272 (BorderUAS) and from the Ministry of Science, Education, and Technological Development of the Republic of Serbia through grant no. 451-03-68/2022-14/200026.

References

1 P. Malcovati and A. Baschirotto, The Evolution of Integrated Interfaces for MEMS Microphones, *Micromachines*, 2018, **9**, 323.
2 S. A. Zawawi, A. A. Hamzah, B. Y. Majlis and F. Mohd-Yasin, A Review of MEMS Capacitive Microphones, *Micromachines*, 2020, **11**, 484.
3 M. A. Shah, I. A. Shah, D.-G. Lee and S. Hur, Design Approaches of MEMS Microphones for Enhanced Performance, *J. Sens.*, 2019, **2019**, 1–26.
4 J. Chen, L. Liu, Z. Li, Z. Tan, Y. Xu and J. Ma, Single-chip condenser miniature microphone with a high sensitive circular corrugated diaphragm, Technical Digest. MEMS 2002 IEEE International Conference. Fifteenth IEEE International Conference on Micro Electro Mechanical Systems (Cat. No.02CH$_3$7266), 2002, pp. 284–287.
5 M. Ying, Q. Zou and S. Yi, Finite-element analysis of silicon condenser microphones with corrugated diaphragms, *Finite Elem. Anal. Des.*, 1998, **30**, 163–173.
6 M. Fuldner, A. Dehe and R. Lerch, Analytical analysis and finite element simulation of advanced membranes for silicon microphones, *IEEE Sens. J.*, 2005, **5**, 857–863.
7 S. Shubham, Y. Seo, V. Naderyan, X. Song, A. J. Frank, J. T. M. G. Johnson, M. da Silva and M. Pedersen, A Novel MEMS Capacitive Microphone with Semiconstrained Diaphragm Supported with Center and Peripheral Backplate Protrusions, *Micromachines*, 2022, **13**, 22.
8 B. S. Sedighe and A. G. Bahram, A novel MEMS capacitive microphone using spring-type diaphragm, *Microsyst. Technol.*, 2019, **25**, 217–224.
9 M. AbdelGhany, F. Mahvash, M. Mukhopadhyay, A. Favron, R. Martel, M. Siaj and T. Szkopek, Suspended graphene variable capacitor, *2D Mater.*, 2016, **3**, 041005.
10 J. Sun, W. Wang, M. Muruganathan and H. Mizuta, Low pull-in voltage graphene electromechanical switch fabricated with a polymer sacrificial spacer, *Appl. Phys. Lett.*, 2014, **105**, 033103.
11 S. J. Cartamil-Bueno, D. Davidovikj, A. Centeno, A. Zurutuza, H. S. J. van der Zant, P. G. Steeneken and S. Houri, Graphene mechanical pixels for Interferometric Modulator Displays, *Nat. Commun.*, 2018, **9**, 4837.
12 M. C. Lemme, S. Wagner, K. Lee, X. Fan, G. J. Verbiest, S. Wittmann, S. Lukas, R. J. Dolleman, F. Niklaus, H. S. J. van der Zant, G. S. Duesberg and P. G. Steeneken, Nanoelectromechanical Sensors Based on Suspended 2D Materials, *Research*, 2020, **2020**, 8748602.
13 D. Davidovikj, P. H. Scheepers, H. S. J. van der Zant and P. G. Steeneken, Static Capacitive Pressure Sensing Using a Single Graphene Drum, *ACS Appl. Mater. Interfaces*, 2017, **9**, 43205–43210.
14 C. Berger, R. Phillips, A. Centeno, A. Zurutuza and A. Vijayaraghavan, Capacitive pressure sensing with suspended graphene–polymer heterostructure membranes, *Nanoscale*, 2017, **9**, 17439–17449.
15 M. Šiškins, M. Lee, D. Wehenkel, R. van Rijn, T. W. de Jong, J. R. Renshof, B. C. Hopman, W. S. J. M. Peters, D. Davidovikj, H. S. J. van der Zant and P. G. Steeneken, Sensitive capacitive pressure sensors based on graphene membrane arrays, *Microsyst. Nanoeng.*, 2020, **6**, 1–9.
16 I. E. Rosłoń, R. J. Dolleman, H. Licona, M. Lee, M. Šiškins, H. Lebius, L. Madauß, M. Schleberger, F. Alijani, H. S. J. van der Zant and P. G. Steeneken, High-frequency gas effusion through nanopores in suspended graphene, *Nat. Commun.*, 2020, **11**, 6025.
17 X. Fan, F. Forsberg, A. D. Smith, S. Schröder, S. Wagner, M. Östling, M. C. Lemme and F. Niklaus, Suspended Graphene Membranes with Attached Silicon Proof Masses as Piezoresistive Nanoelectromechanical Systems Accelerometers, *Nano Lett.*, 2019, **19**, 6788–6799.
18 Q. Zhou, J. Zheng, S. Onishi, M. F. Crommie and A. K. Zettl, Graphene electrostatic microphone and ultrasonic radio, *Proc. Natl. Acad. Sci. U. S. A.*, 2015, **112**, 8942–8946.
19 S. Wittmann, C. Glacer, S. Wagner, S. Pindl and M. C. Lemme, Graphene Membranes for Hall Sensors and Microphones Integrated with CMOS-Compatible Processes, *ACS Appl. Nano Mater.*, 2019, **2**, 5079–5085.
20 D. Todorović, A. Matković, M. Milićević, D. Jovanović, R. Gajić, I. Salom and M. Spasenović, Multilayer graphene condenser microphone, *2D Mater.*, 2015, **2**, 045013.
21 G. S. Wood, A. Torin, A. K. Al-mashaal, L. S. Smith, E. Mastropaolo, M. J. Newton and R. Cheung, Design and Characterization of a Micro-Fabricated GrapheneBased MEMS Microphone, *IEEE Sens. J.*, 2019, **19**, 7234–7242.
22 S. Woo, J.-H. Han, J. H. Lee, S. Cho, K.-W. Seong, M. Choi and J.-H. Cho, Realization of a High Sensitivity

Microphone for a Hearing Aid Using a Graphene–PMMA Laminated Diaphragm, *ACS Appl. Mater. Interfaces*, 2017, **9**, 1237–1246.

23 J. Xu, G. S. Wood, E. Mastropaolo, M. J. Newton and R. Cheung, Realization of a Graphene/PMMA Acoustic Capacitive Sensor Released by Silicon Dioxide Sacrificial Layer, *ACS Appl. Mater. Interfaces*, 2021, **13**, 38792–38798.

24 H. M. Mustapha, M. F. M. R. Wee, A. R. M. Zain and M. A. Moahmed, Characterization of Graphene based Capacitive Microphone, *Sains Malays.*, 2019, **48**, 1201–1207.

25 J. Xu, G. S. Wood, A. K. Al-mashaal, E. Mastropaolo, M. J. Newton and R. Cheung, Realization of Closed Cavity Resonator Formed by Graphene-PMMA Membrane for Sensing Audio Frequency, *IEEE Sens. J.*, 2020, **20**, 4618–4627.

26 S. Vollebregt, B. Alfano, F. Ricciardella, A. J. M. Giesbers, Y. Grachova, H. W. van Zeijl, T. Polichetti and P. M. Sarro, A transfer-free wafer-scale CVD graphene fabrication process for MEMS/NEMS sensors, 2016 IEEE 29th International Conference on Micro Electro Mechanical Systems (MEMS), 2016.

27 B. Vasić, U. Ralević, K. Cvetanović Zobenica, M. Smiljanić, R. Gajić, M. Spasenović and S. Vollebregt, Low-friction, wear-resistant, and electrically homogeneous multilayer graphene grown by chemical vapor deposition on molybdenum, *Appl. Surf. Sci.*, 2020, **509**, 144792.

28 T. Gabrielson, Mechanical-thermal noise in micromachined acoustic and vibration sensors, *IEEE Trans. Electron Devices*, 1993, **40**, 903–909.

29 Z. Li, I. A. Kinloch, R. J. Young, K. S. Novoselov, G. Anagnostopoulos, J. Parthenios, C. Galiotis, K. Papagelis, C.-Y. Lu and L. Britnell, Deformation of Wrinkled Graphene, *ACS Nano*, 2015, **9**, 3917–3925.

30 Invensense, *Microphone specifications explained Application Note AN-1112*, 2016.

31 STMicroelectronics, *MP23DB01HP Datasheet MEMS audio sensor: digital microphone with multiple performance modes*, 2021.

32 P. R. Scheeper, A. G. H. van der Donk, W. Olthuis and P. Bergveld, A review of silicon microphones, *Sens. Actuators, A*, 1994, **44**, 1–11.

33 D. Davidovikj, F. Alijani, S. J. Cartamil-Bueno, H. S. J. van der Zant, M. Amabili and P. G. Steeneken, Nonlinear dynamic characterization of two-dimensional materials, *Nat. Commun.*, 2017, **8**, 1253.

34 A. K. Al-mashaal, G. S. Wood, A. Torin, E. Mastropaolo, M. J. Newton and R. Cheung, Dynamic behavior of ultra large graphene-based membranes using electrothermal transduction, *Appl. Phys. Lett.*, 2017, **111**, 243503.

35 Y. She, C. Li, T. Lan, X. Peng, Q. Liu and S. Fan, The Effect of Viscous Air Damping on an Optically Actuated Multilayer MoS2 Nanomechanical Resonator Using Fabry-Perot Interference, *Nanomaterials*, 2016, **6**, 162.

36 M. Fueldner, *Handbook of Silicon Based MEMS Materials and Technologies – Microphones*, Elsevier, 2020, pp. 937–948.

37 R. Pezone, G. Baglioni, P. M. Sarro, P. Steeneken and S. Vollebregt, Sensitive transferfree wafer-scale graphene microphones, *ACS Appl. Mater. Interfaces*, 2022, **14**(18), 21705–21712.

38 S. Wagner, C. Weisenstein, A. D. Smith, M. Östling, S. Kataria and M. C. Lemme, Graphene transfer methods for the fabrication of membrane-based NEMS devices, *Microelectron. Eng.*, 2016, **159**, 108–113.

39 M. Bao and H. Yang, Squeeze film air damping in MEMS, *Sens. Actuators, A*, 2007, **136**, 3–27.

